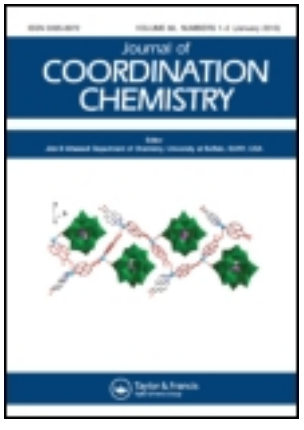

Journal of Coordination Chemistry
Publication details, including instructions for authors and subscription information:
http://www.tandfonline.com/loi/gcoo20

Effect of 1,10-phenanthroline on DNA binding, DNA cleavage, cytotoxic and lactate dehydrogenase inhibition properties of Robson type macrocyclic dicopper(II) complex

Sellamuthu Anbu[a], Asaithambi Killivalavan[b], Elisabete C.B.A. Alegria[cd], Ganeshan Mathan[b] & Muthusamy Kandaswamy[a]

[a] Department of Inorganic Chemistry, School of Chemical Sciences, University of Madras, Guindy Maraimalai Campus, Chennai, India

[b] Department of Biomedical Science, School of Basic Medical Sciences, Bharathidasan University, Tiruchirapalli, India

[c] Chemical Engineering Departmental Area, ISEL, Lisboa, Portugal

[d] Centro de Química Estrutural, Complexo I, Instituto Superior Técnico, Technical University of Lisbon, Lisboa, Portugal

Accepted author version posted online: 24 Oct 2013.Published online: 26 Nov 2013.

To cite this article: Sellamuthu Anbu, Asaithambi Killivalavan, Elisabete C.B.A. Alegria, Ganeshan Mathan & Muthusamy Kandaswamy (2013) Effect of 1,10-phenanthroline on DNA binding, DNA cleavage, cytotoxic and lactate dehydrogenase inhibition properties of Robson type macrocyclic dicopper(II) complex, Journal of Coordination Chemistry, 66:22, 3989-4003, DOI: 10.1080/00958972.2013.858136

To link to this article: http://dx.doi.org/10.1080/00958972.2013.858136

Journal of Coordination Chemistry, 2013
Vol. 66, No. 22, 3989–4003, http://dx.doi.org/10.1080/00958972.2013.858136

Effect of 1,10-phenanthroline on DNA binding, DNA cleavage, cytotoxic and lactate dehydrogenase inhibition properties of Robson type macrocyclic dicopper(II) complex

SELLAMUTHU ANBU*†, ASAITHAMBI KILLIVALAVAN‡, ELISABETE C.B.A. ALEGRIA§¶, GANESHAN MATHAN‡ and MUTHUSAMY KANDASWAMY*†

†Department of Inorganic Chemistry, School of Chemical Sciences, University of Madras, Guindy Maraimalai Campus, Chennai, India
‡Department of Biomedical Science, School of Basic Medical Sciences, Bharathidasan University, Tiruchirapalli, India
§Chemical Engineering Departmental Area, ISEL, Lisboa, Portugal
¶Centro de Química Estrutural, Complexo I, Instituto Superior Técnico, Technical University of Lisbon, Lisboa, Portugal

(*Received 10 August 2013; accepted 10 October 2013*)

DNA targeting macrocyclic dicopper(II) complex, $[Cu_2L(H_2O)_2](phen)_2(ClO_4)_2$ (*L* = μ-11, 23-dimethyl-3,7,15,19-tetraazatricyclo-[19.3.1.1^{9,13,21}] he p t a c o s a-1(24), 2, 7, 9, 11, 13(26), 14, 19, 21(25), 22-decaene-25,26-diol) (**2**), has been synthesized and characterized. This has been synthesized by reacting a Robson type macrocyclic precursor dicopper(II) complex $[Cu_2L(H_2O)_2](ClO_4)_2$ (**1**) and 1,10-phenanthroline in ethanol. Solution ESR, electronic, and ESI-MS spectral studies suggest that 1,10-phenanthroline replaces coordinated water in **1**, giving **2**. The influence of the phenanthroline on DNA binding, cleavage, and anticancer properties of **2** have been investigated. Complex **2** displays better DNA binding and cleavage than **1**. The dicopper(II) complexes **1** and **2** show cytotoxicity in human cervical HeLa cancer cells, giving IC_{50} values of 79.41 and 15.82 μM, respectively. Antiproliferative properties of **1** and **2** were confirmed by Trypan Blue exclusive assay and lactate dehydrogenase enzyme level in HeLa cancer cell lysate and content media.

Keywords: Dicopper(II) complexes; DNA binding and cleavage; Trypan Blue assay; Anticancer properties; LDH inhibition

1. Introduction

The development of new reagents that can specifically bind and cleave DNA under physiological conditions via oxidative and hydrolytic mechanisms has attracted considerable interest due to applications in cancer therapy and molecular biology [1–4]. Platinum complexes are well-known metal-based drugs for cancer therapy. However, it possesses inherent limitations such as side effects and resistance phenomena [5, 6]. This leads to search for other metal complexes for cancer therapy with distinctive cellular apoptotic pathways.

*Corresponding authors. Email: bioinorg_anbu@yahoo.com (S. Anbu); mkands@yahoo.com (M. Kandaswamy)

Copper(II) plays a significant role in biological systems as pharmacological and physiological agents [7, 8]. Several Cu(II) complexes have been reported as potential anticancer agents, active in both *in vitro* and *in vivo* [9–11]. Several phenanthroline based mononuclear Cu(II) complexes were synthesized and their interactions with DNA and cytotoxic activities [7, 12–14] were reported. These studies are mainly limited to mononuclear complexes and very few studies on dinuclear complexes with metal ions in close proximity were reported [15, 16]. Recently, we have synthesized phenanthroline based dicopper(II) complexes, which strongly bind to DNA and also regulate apoptosis [17, 18]. We also have reported some macrocyclic and macrobicyclic dinuclear complexes with more aromaticity show better DNA interaction, nuclease, and anticancer activity than the dinuclear analogs with aliphatic moieties [19–25]. In this context, we have synthesized the 1,10-phenanthroline containing Robson type symmetrical macrocyclic dicopper(II) complex **2** for DNA binding, cleavage, and primary anticancer properties; results are compared with the 1,10-phenanthroline free macrocyclic dicopper(II) complex **1**.

2. Experimental

2.1. *Materials and measurements*

Robson type macrocyclic dicopper(II) complex **1** has been synthesized as described [26]. Copper(II) perchlorate hexahydrate, 1,10-phenanthroline, and ethidium bromide (EB) were purchased from Aldrich. Calf thymus DNA (CT–DNA) and pBR322DNA were purchased from Bangalore Genei (India). All other chemicals and solvents were of analytical grade and used as received. Elemental analysis was carried out on a Carlo Erba model 1106 elemental analyzer. The percentage of Cu in a complex was determined using a Perkin–Elmer AAS (model 2380) equipped with a hollow cathode source and employing air/acetylene flame. FT-IR spectra were obtained on a Perkin–Elmer FTIR spectrometer with samples prepared as KBr pellets. UV–vis spectra were recorded using a Perkin-Elmer Lambda 35 spectrophotometer operating from 200 to 1100 nm with quartz cells; ε are given in M^{-1} cm^{-1}. Electrospray ionization mass spectral measurements were done using a Thermo Finnigan LCQ-6000 Advantage Max-ESI mass spectrometer. Both room temperature (RT) and liquid nitrogen temperature (LNT) solid/solution ESR spectra of **1** and **2** were recorded using a JEOL TES 100 ESR spectrometer. Diphenyl picryl hydrazyl was used as the field marker.

Caution! Transition metal perchlorate salts are potentially explosive; hence, care should be taken in handling the compound!

2.2. *Synthesis of dicopper(II) complex $[Cu_2L(H_2O)_2](phen)_2(ClO_4)_2$ (2)*

Slow addition of $LiOH{\cdot}H_2O$ (0.04 g, 1.00 mM) in water (3 mL) to **1** (0.38 g, 0.5 mM) in ethanol (10 mL) produces a yellowish green solution. Then, ethanolic solution (7 mL) of 1,10-phenanthroline (0.18 g, 1 mM) was added dropwise under constant stirring. The above reaction mixture was refluxed for 12 h and then the solution was concentrated to about 5 mL by evaporation of the solvent under reduced pressure. By slow cooling to RT of the resulting solution, a brown solid was separated by filtration. Recrystallization from acetonitrile solution offered yellowish green crystals suitable for single crystal XRD analysis.

Yield: 2.30 g (75%) Anal. Calcd for $C_{48}H_{42}Cl_2Cu_2N_8O_{10}$ (**2**) Calcd: C, 52.94; H, 3.89; N, 10.29; Cu, 11.67%. Found: C, 52.98; H, 3.92; N, 10.34; Cu, 11.76%. ESI-MS in CH_3CN: *m/z* 444.54 $[M–2ClO_4]^{2+}$. FT-IR, cm^{-1} (KBr disk): 3214 [w, *ν*(N–H)], 1636 [w, *ν*(C=N)], 1365 [s, *ν*(C–O)], 1092vs, 625s [$\nu(ClO_4^-)$], 492 [w, *ν*(Cu–N)] (br, broad; s, strong; w, weak). $\lambda_{max,}$ nm (ϵ, M^{-1} cm^{-1}) in CH_3CN: 684 (98), 375 (6000), 263 (77,900), 227 (128,000); g at 298 K = 2.074; μ_{eff}, μ_B at 298 K: 1.21 BM.

2.3. *X-ray data collection and reduction*

Crystals of **2** were translucent green and could be sorted by using a polarizing microscope (Leica DMLSP). The crystal was cut into suitable size and mounted on a Kappa Apex2 CCD diffractometer equipped with graphite monochromated Mo(Kα) radiation (λ = 0.71073 Å). The intensity data were collected using ω and φ scans with frame width of 0.5°. The frame integration and data reduction were performed using Bruker SAINT-Plus (Version 7.06a) software [27]. Multi-scan absorption corrections were applied using SADABS (Bruker, 1999) [28]. The structure was solved using SIR92 [29]. Full matrix least squares refinement was performed using SHELXL-97 (Sheldrick, 1997) programs. All non-hydrogen atoms were refined with anisotropic displacement parameters. Refinement of water hydrogens were restrained such that they remain in the vicinity of the respective difference peak. All hydrogens could be located in the difference Fourier map. However, they were relocated at chemically meaningful positions and were given riding model refinement with the following restraints: tertiary CH_3 groups (C–H = 0.96 Å, U_{iso} = 1.5 U_{eq} of the parent carbon), secondary CH_2 group (C–H = 0.97 Å, U_{iso} = 1.2 U_{eq} of the parent carbon), and aromatic C–H group (C–H = 0.93 Å U_{iso} = 1.2 U_{eq} of the parent carbon). The water hydrogens were restrained such that they remain in the vicinity of the respective difference peak. Selected crystallographic data of **2** are given in table 1.

Table 1. Crystallographic data for **2**.

Parameters	**2**
Empirical formula	$C_{48}H_{46}Cl_2Cu_2N_8O_{12}$
Formula weight	1124.91
T (K)	293(2)
Wavelength (Å)	0.71073
Crystal system	Monoclinic
Space group	$P2_1/c$
a (Å)	7.2055(2)
b (Å)	25.4986(9)
c (Å)	13.2132(5)
α (°)	90
β (°)	102.699(2)
γ (°)	90
Volume ($Å^3$)	2368.28(14)
Z	2
Calculated density (mg m^{-3})	1.577
Absorption coefficient (mm^{-1})	1.085
Crystal size (mm)	0.30 × 0.20 × 0.20
θ Range for data collection (°)	2.25–24.81
Max. and min. transmission	0.737 and 0.812
Data/restraints/parameters	4880/5/338
Final *R* indices [I > 2σ(I)]	R_1 = 0.0481(3667)
R indices (all data)	wR_2 = 0.1539(4880)
Largest diff. peak and hole (e.$Å^{-3}$)	0.778 and –0.766

2.4. *MTT assay*

Human cervical carcinoma HeLa cell line was obtained from National Center for Cell Science (NCCS), Pune, India and cell viability was assessed by MTT (3,4,5-dimethylthiazolyl-2-2,5-diphenyltetrazolium bromide) method. HeLa cells were maintained in a humidified atmosphere containing 5% CO_2 at 37 °C in Dulbecco's Modified Eagle's Medium supplemented with 100 units of penicillin, 100 μg mL^{-1} of streptomycin, and 10% Fetal bovine serum. Briefly, HeLa cells with a density 1×10^4 cells per well were precultured in 96-well microtiter plates for 24 h under 5% CO_2. **1** and **2** were added in micro wells containing the cell culture at 2–100 μM, and then each well was loaded with 10 μL MTT solution (5 mg mL^{-1} in phosphate buffered saline (PBS) pH = 7.4) for 4 h at 37 °C. The insoluble formazan was dissolved in 100 μL of 4% DMSO and the cell viability was determined by measuring the absorbance of each well at 570 nm using a Bio-Rad 680 microplate reader (Bio-Rad, USA). All experiments were performed in triplicate and the percentage of cell viability was calculated according to the equation, inhibition rate (%) = OD (control) – OD (drug treated cells)/OD (control) × 100.

2.5. *Trypan Blue exclusion assay*

Viability assays measure the percentage of a cell suspension that is viable. This method is based on the principle that live (viable) cells do not take up certain dyes whereas dead (non-viable) cells do. Live cells with intact cell membranes are not colored. Because cells are very selective in the compounds that pass through the membrane, in a viable cell, Trypan Blue is not absorbed; however, it traverses the membrane in a dead cell. Therefore, dead cells are shown as a distinctive blue color under a microscope. For the Trypan Blue assay, HeLa cells were seeded into 24-well plates at a density of $1–2 \times 10^5$ cells/well with different concentrations of **1** and **2**. After 24 h, cells were harvested by trypsinization (trypsin 0.025%/EDTA 0.02%) before incubating with 0.4% Trypan Blue solution in PBS for 2 min. Cells were allowed to stand from 5 to 15 min. Later, 10 μL of stained cells were placed in a hemocytometer, and the number of viable (unstained) and dead (stained) cells was counted with a light microscope. The viability percentage was expressed using the equation, cell viability (%) = total viable cells (unstained)/total cells (stained and unstained) × 100. Representative measurements of three distinct sets of data have been reported.

2.6. *Lactate dehydrogenase inhibition assay*

Glycine buffer (0.1 M) (pH 7.4), buffered substrate (lithium lactate in NaOH), nicotinamide adenine dinucleotide (NAD^+) (5 mg mL^{-1}), 0.02% dinitro phenyl hydrazine (DNPH) in 1 N HCl, 0.4 N NaOH, and stock standard Tri sodium pyruvate were purchased from Genei India. Lactate dehydrogenase (LDH) assay was measured in both cell lysate and in the conditioned medium. After 48 h incubation, the culture medium with treatment was taken separately and the attached cells were lysed by adding 0.1% triton × 100 and subjecting them to two cycles of freezing and thawing. The activity of LDH was measured by following King's method [30]. The substrate reaction buffer containing 0.5 mM lactic acid, 0.1 N NaOH, and 0.1 M glycine buffer was added to the cell lysate and medium and then 0.02 mL of NAD was added to both. Dinitro phenyl hydrazine (0.02%) was added as chromogenic agent and the absorbance values at 460 nm were read in the UV spectrophotometer. The units were expressed in μM of pyruvate liberated/protein (μg). The

percentage of LDH leakage was expressed using the equation, percentage of leakage of LDH = activity in medium/activity in cells + activity in medium × 100. Representative measurements of three distinct sets of data have been reported.

3. Results and discussion

3.1. *General properties*

A very strong band near 1100 cm^{-1} and a strong and sharp band near 625 cm^{-1} are observed in IR spectra of **1** and **2** (figure S1, Supplementary material), in agreement with the presence of uncoordinated perchlorate ions in their crystal lattices [31]. The ν(O–H) of coordinated water in **1** is a broad band at 3480 cm^{-1} [32], which is absent in **2** attributed to coordination of 1,10-phenanthroline by replacing water. Complex **2** shows a band at 1638 cm^{-1} due to ν(C=N), which is less intense than for **1**. This is attributed to coordination of 1,10-phenanthroline to Cu(II) ion in **2** by replacing one azomethine from each compartment of the macrocyclic ring. To ascertain structural changes of **1** and **2** in different phases, solid and solution electronic spectra of the complexes (figure S2, Supplementary material) were recorded. The reflectance spectra of **1** and **2** (figure S2B) show an asymmetrical absorption at 600 and 595 nm, respectively, related to d–d transitions. The identical feature (figure S2C) is observed around at 600 nm for **1** in different solvents (table S1), suggesting that the molecular structure of **1** is maintained under these experimental conditions [33]. The phenanthroline containing **2** in different solvents has a new d–d band around 690 nm (figure S2D), entirely different from the reflectance spectra of **2**, but comparable to reported phenanthroline coordinated mixed ligand Cu(II) complexes [34–36]. These results strongly support that the structure of phenanthroline containing **2** in solution is not the same as in the solid state. The positive ion ESI mass spectrum (figure S3, Supplementary material) of **2** in CH_3CN showed major peaks at m/z = 444.54 and 990.27 corresponding to $[M–2ClO_4]^{2+}$ and $[M–ClO_4]^{+}$, respectively. The analytical and ESI mass spectral data of **2** also strongly support coordination of phenanthroline to Cu(II) by replacing coordinated water in solution. To corroborate the coordination environments around Cu(II), solid and solution ESR spectra of **1** and **2** were recorded at RT and LNT. ESR spectral data for the complexes are listed in table S1, Supplementary material. At both RT and LNT, polycrystalline samples of **1** and **2** showed a single broad-band ESR spectrum and the observed g values are 2.040–2.074, but **1** and **2** in CH_3CN show four lines with nuclear hyperfine spin 3/2 due to hyperfine splitting at RT and LNT (figure S4, Supplementary material). The observed $g_{\|}$, $g_{\perp}$, and $A_{\|}$ values for **1** were 2.247−2.272, 2.07−2.11, and 179−182 × 10^{-4} cm^{-1}, respectively, typical of a water (axially) coordinated square-pyramidal N,O-donor copper(II) complex [37]. At identical temperatures, **2** also exhibited typical four-line splitting patterns with $g_{\|}$ = 2.102−2.124, $g_{\perp}$ = 2.02−2.05, and $A_{\|}$ = 168−172 × 10^{-4} cm^{-1}. The distorted square-pyramidal phenanthroline free **1** shows the $A_{\|}$ of 180 × 10^{-4} cm^{-1}, while phenanthroline coordinated macrocyclic dicopper(II) **2** exhibits the $A_{\|}$ value around 170 × 10^{-4} cm^{-1}. This decrease of $A_{\|}$ for **2** reveals different coordination environments around Cu(II). Distortion of square-pyramidal geometry toward trigonal-bipyramidal geometry causes reduction in $A_{\|}$ [38, 39], and the difference in $A_{\|}$ between **1** and **2** is believed to originate from this structural factor. Coordination of 1, 10-phenanthroline to Cu(II) by removing water led to different geometry around Cu(II)

centers in solution. RT magnetic studies of **1** and **2** resulted in magnetic moment value of 1.23 and 1.21 BM. Both ESR and magnetic studies of complexes suggest the presence of an antiferromagnetic interaction between Cu(II) ions.

3.2. *Crystal structure of $[Cu_2L(H_2O)_2](phen)_2(ClO_4)_2$ (2)*

Complex **2** crystallized in the monoclinic lattice with a space group $P2_1/c$. The molecular structure of **2** is shown in figure 1. The coordination geometry around the two coppers in **2** is the same as that in **1** [26], with two waters occupying two axial positions at the opposite side of the macrocyclic plane. Copper(II) is situated slightly above the N_2O_2 plane and each metal may be considered as distorted square-pyramidal. Two nitrogens from two 1,10-phenanthrolines are linked to two coordinating water molecules above and below the macrocyclic framework, through hydrogen bonds. The hydrogens of coordinated water could not be located. However, the distance (2.780 Å) between oxygen of water (O1) and N4_$1 ($1 = $-x$, ½ + y, ½ − z) shows strong hydrogen bond interaction between 1,10-phenanthroline and macrocyclic dicopper(II) complex. Two hydrogen bonded phenanthroline rings are found in almost parallel positions to the phenyl ring in the macrocyclic plane (with a dihedral angle of 6.3°). They lie face–to–face with the adjacent macrocyclic frameworks on their other side. The two phenanthroline rings situated between two macrocycles are strictly coplanar to each other (with a dihedral angle of 0.0°), forming an ordered arrangement where one macrocycle and two 1,10-phenanthrolines are alternately arrayed (figure S5, Supplementary

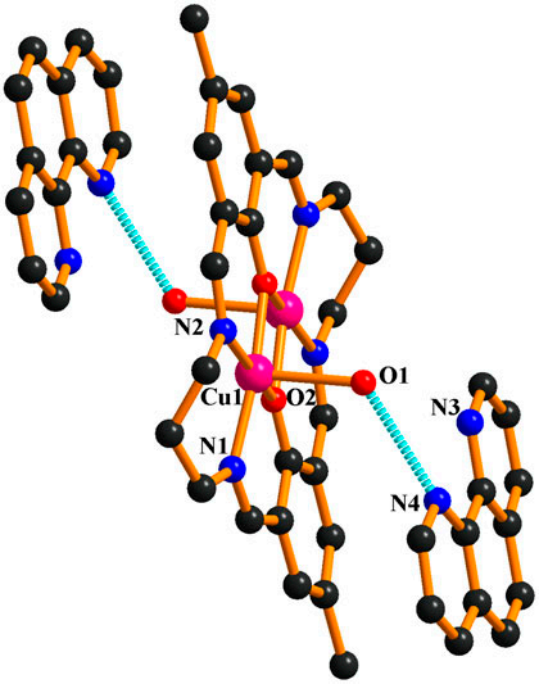

Figure 1. Crystal structure of **2**. Hydrogens and perchlorates are omitted for clarity.

material). The separations between the macrocyclic and phenanthroline rings are about 3.6 Å. It is proposed that π–π interactions are present between phenanthroline and phenyl in the macrocyclic skeleton, where the electron-rich phenanthroline moiety (uncoordinated) is a donor and the electron-poor phenyl species (owing to the coordination of the macrocyclic) as acceptors. It is suggested that both the π–π interactions and H-bonding interactions contribute to the stacking structure.

3.3. *DNA binding and cleavage properties*

3.3.1. Absorption spectral studies. The binding ability of **1** and **2** with CT–DNA was studied by measuring their effects on the electronic spectra. Interaction of **1** and **2** in DMF solutions (5%) with CT–DNA was investigated. Absorption titration experiments in buffer were performed using a fixed copper concentration to which increments of the DNA stock solution were added. The binding of Cu^{II} complexes to duplex DNA led to a decrease in absorption intensities with small red shifts in the UV–vis absorption spectra [40]. To compare quantitatively the affinity of the two complexes toward DNA, the binding constants K of the two complexes to CT–DNA were determined by monitoring the changes of absorbance (figure 2) at 253 and 350 nm for **1** and 263 and 227 nm for **2**), with increasing concentration of DNA [41]. The intensity of the intraligand π–π* transitions decreases with increase of CT–DNA, indicating interactions exist between DNA and **1** or **2**. However, the influence of **2** on the UV–vis spectra is greater than that of **1**. Complex **2** shows significant bathochromic shift of ~4 nm suggesting a groove-binding preference of the complex. The intrinsic equilibrium DNA binding constant (K_b) values of the complexes along with the binding site size (s) are given in table 2. The binding site size (s) values were obtained from the MvH fits and **2** has a higher value of s in comparison to **1**. The K_b values are lower than for a classical intercalator (e.g. EB-DNA, ~10^6 M^{-1}) [42] and are close to those of DNA-intercalative dicopper(II) complexes [43–47], but higher than those of mononuclear copper (II) complexes [48–50], indicating that **2** provides more aromatic moiety to overlap with the stacking base pairs of the DNA helix by major groove binding, which results in hypochromism and bathochromism. The increasing aromaticity of **2** facilitates its major groove DNA binding, while **1** may prefer electrostatic interaction.

3.3.2. Circular dichroism studies. The observed circular dichroism (CD) spectrum of CT–DNA consists of a positive band at 278 nm due to base stacking and a negative band at 245 nm due to helicity, characteristic of DNA in the right handed B form [51, 52]. Groove binding and electrostatic interaction of small molecules with DNA show little or no perturbations on the base stacking and helicity bands. The CD spectra of DNA taken after incubation of the complexes with CT–DNA are shown in figure S6, Supplementary material. Examination of figure S6 shows that the magnitude of the elipticity at 274 nm increases **1** < **2**. This suggests that the DNA binding of **2** induces conformational changes, such as the conversion from a more B–like to a more C–like structure within the DNA molecule [53]. These changes are indicative of a non-intercalative mode of binding and support their groove binding nature [54].

3.3.3. Fluorescence spectral studies. Fluorescence is effective to study the metal interaction with DNA. EB is one of the most sensitive fluorescence probes that can bind with

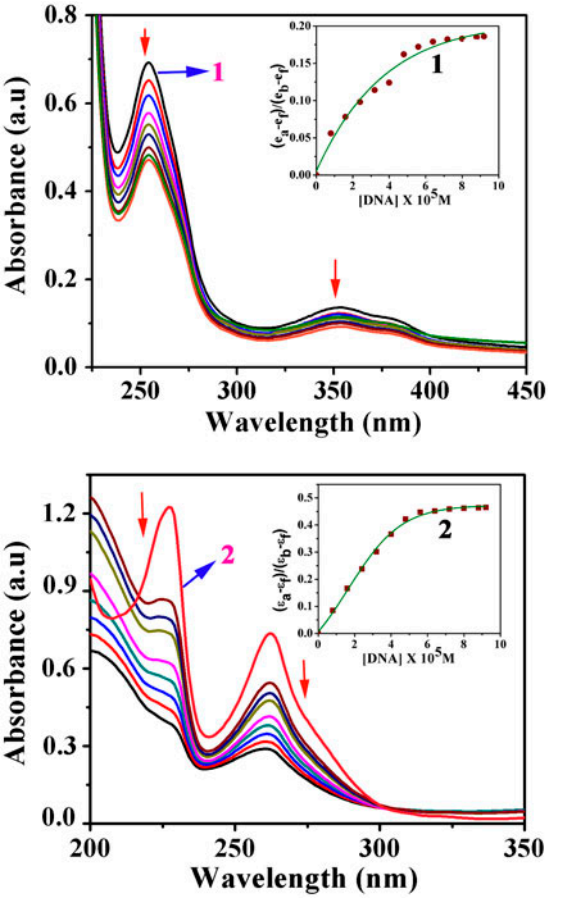

Figure 2. Absorption spectral traces of **1** and **2** in 50 mM Tris-HCl/NaCl buffer (pH = 7.5) on increasing quantity of CT–DNA. Arrow shows the absorbance changing upon increasing DNA concentrations. Insets show the plot of $(\varepsilon_a - \varepsilon_f)/(\varepsilon_b - \varepsilon_f)$ *vs.* [DNA] for the titration of DNA to the dicopper(II) complexes **1** and **2**.

Table 2. DNA binding, cleavage and cytotoxicity parameters of **1** and **2**.

	DNA binding, cleavage and cytotoxicity				
Complex	$10^5\ K_b$ [s][a] (M^{-1})	$10^5\ K_{app}$[b] (M^{-1})	$10^{-5}\ K_M$ (M)	$10^{-2}\ k_{cat}$ (h^{-1})	IC_{50}[c] (μM)
1	2.95 [0.55]	3.11	2.34	1.83	79.41
2	5.35 [1.12]	7.81	5.72	2.72	15.82

[a]Binding constants (M^{-1}) were determined by absorption spectrophotometric titration and [s] is the binding site size of DNA in base pairs.
[b]Apparent binding constants (M^{-1}) were determined by fluorescence spectrophotometric method.
[c]IC_{50} (μM) values were determined by MTT assay by exposing HeLa cells with different concentrations of **1** and **2** for 24 h.

DNA [55]. The fluorescence of EB increases after intercalating into DNA. If the metal intercalates into DNA, it leads to a decrease in the binding sites of DNA available for EB, resulting in decrease in the fluorescence intensity of the EB–DNA system [42]. Emission spectra of EB bound to DNA in the absence and presence of **1** and **2** are shown in figure

S7, Supplementary material. The addition of the complex to DNA pretreated with EB causes appreciable reduction in fluorescence intensity, indicating that **1** and **2** compete with EB to bind to DNA. The reduction of the emission intensity gives a measure of the DNA binding propensity of the complexes and stacking interaction between the adjacent DNA base pairs [56]. The fluorescence quenching curve of DNA–bound EB by **1** and **2** illustrates that quenching of EB bound to DNA by **1** and **2** is in agreement with the linear Stern–Volmer equation ($I_0/I = 1 + K_{SV}[Q]$), where I_0 and I are the fluorescence intensities of the CT–DNA in the absence and presence of **1**, respectively. K_{SV} is the Stern–Volmer dynamic quenching constant and [Q] is the total concentration of the quencher (in this case, **1** and **2**). In the linear fit plot of I_0/I *versus* [complex]/[DNA], K is given by the ratio of the slope to the intercept. The K_{SV} values for **1** and **2** are 7.26 (R = 0.992) and 10.2 (R = 0.984), respectively. The concentrations of the complexes are taken for observing 50% reduction (figure S7B) of emission intensity of EB [57]. It is also known that 50% of EB molecules were replaced from DNA–bound EB at a concentration ratio of $[Cu_2Complex]/[EB] = K_1$. The K_1 values of **1** and **2** were 32.2 and 12.8, respectively. By taking a DNA binding constant of 1.0×10^7 M^{-1} for EB [58], apparent DNA binding constants K_{app} of the complexes (table 2) were derived from the equation (K_b(EB)/K_1). The K_{app} values imply that **1** and **2** strongly interact with DNA and are protected by DNA efficiently since the hydrophobic environment inside the DNA helix reduces the accessibility of solvent water to the complex and the complex mobility is restricted at the binding site [59]. The interaction of phenanthroline ring and also the hydrophobic property of the rigid macrobicyclic ligand also facilitate DNA binding [60].

3.3.4. Viscosity measurements. To clarify the binding of **1** and **2** with DNA, viscosities of DNA solutions containing varying amounts of added complexes were measured. Since the relative specific viscosity (η/η_0) of DNA gives a measure of the increase in contour length associated with separation of DNA base pairs caused by intercalation, a classical DNA intercalator like EB shows a significant increase in the viscosity (figure 3) of the DNA solutions (η and η_0 are the specific viscosities of DNA in the presence and absence of the complexes, respectively). In contrast, a partial and/or non-intercalation of the complex could result in less pronounced effect on the viscosity [61]. The groove binder Hoechst 33258 has been used as a reference compound that shows almost no apparent change in viscosity. The results indicate that **2** is possibly DNA groove binder [62] and **1** can bind to DNA through electrostatic interactions only, because it exerted essentially no such effect.

3.3.5. DNA cleavage activity. The DNA cleavage activity of **1** and **2** has been studied using SC pBR322 DNA in Tris-HCl/NaCl buffer (pH 7.2) in the dark. The results of the gel electrophoresis separations of plasmid pBR322 DNA by **1** and **2** are depicted in figure 4. A 20 μM solution of **1** shows significant cleavage (Lane 3) of SC DNA (0.33 μg) on 3 h incubation at 37 °C. Under similar conditions, free pBR322 DNA, H_2O_2, or **2** does not show cleavage (Lanes 1, 2 and 4). Complex **2** on reaction with DNA in the presence of H_2O_2 as oxidizing agent displayed remarkable nuclease activity (Lane 5). At a slightly higher concentration of the dinuclear complexes (30 μM) the cleavage is found to be much more efficient, shown by formation of more nicked circular (NC) form (Form II) in Lanes 5 and 6. The mechanistic aspects of the DNA cleavage reactions of **1** and **2** have been studied using different additives (figure S8, Supplementary material). In the presence of hydroxyl radical

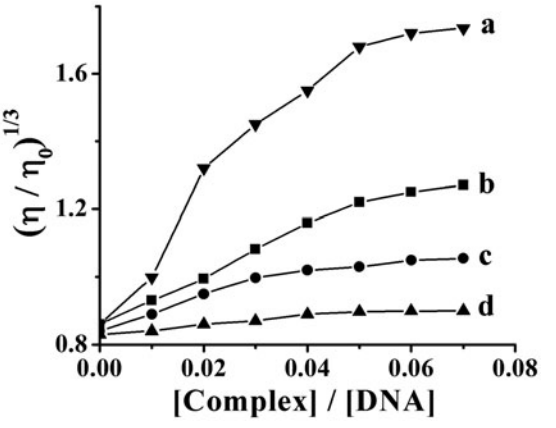

Figure 3. Effect of increasing amounts of EB (a), **2** (b), **1** (c), and Hoechst 33258 (d) on the relative viscosity of CT–DNA at 25 (±0.1) °C. The total concentration of DNA is 0.5 mM.

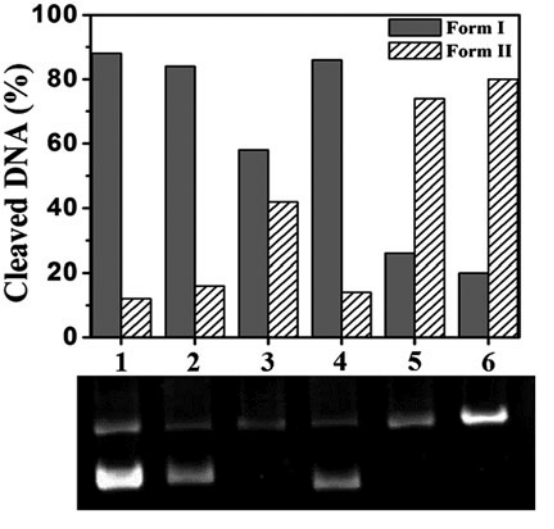

Figure 4. Cleavage of SC pBR322 DNA (0.2 μg, 33.3 μM) by **1** and (20–30 μM) in 50 mM Tris-HCl/NaCl buffer (pH 7.5). Lane 1, DNA control; Lane 2, DNA + H_2O_2 (40 μM); Lanes 3 and 4, DNA + **1** and **2** (20 μM); Lane 5, DNA + **1** (30 μM); Lane 6, DNA + **2** (30 μM) + H_2O_2 (40 μM).

scavengers, **1** does not show significant inhibition of the DNA cleavage. The oxygen-independent hydrolytic cleavage pathway under an argon atmosphere suggests that the cleavage activity of **1** does not involve an oxidative process. These results reveal that **1** can cleave DNA through hydrolytic pathway by using Cu^{II} coordinated water molecules [19, 63]. Whereas **2** displays oxidative mode of DNA cleavage attribute to the absence of axially coordinated water. Complex **2** is cleavage inactive under argon atmosphere, indicating the necessity of reactive oxygen species (ROS) for the DNA cleavage. Hydroxyl radical scavengers like DMSO also show complete inhibition in the DNA cleavage. The results suggest that the

involvement of hydroxyl radicals as ROS. In the presence of H_2O_2, **2** displays an oxygen dependent nuclease activity using $OH^{\bullet}$ as reactive species. Copper(II) coordinated 1,10-phenanthroline molecules drastically alter the mode of DNA degradation properties of macrocyclic complexes.

The kinetic aspect of the DNA cleavage (figure 5) by **1** and **2** vary exponentially with incubation time and follows pseudo-first-order kinetics. Kinetic plots showing the formation of NC DNA and the degradation of SC DNA *versus* time follow pseudo-first-order kinetics and they fit well to a single exponential curve (figure S9, Supplementary material). Based on the plots of k_{obs} *versus* concentrations of complex, the pseudo-Michaelis–Menten kinetic parameters for **1** and **2** were determined and are summarized in table 2. Under similar reaction conditions, dicopper(II) complex, reported by Rossi and coworkers [64] as a "chemical nuclease," displayed significantly less cleavage activity in comparison to **1** and **2**. Complex **2** also shows two times faster cleavage rate than **1**. The rate of DNA hydrolysis enhancement by **1** is comparable to those reported for transition metal-based hydrolases but less when compared to Mg–EcoRV or Mn–EcoRV (~1.3×10^9) [10, 58, 65–67].

3.4. *Cytotoxic analysis*

3.4.1. MTT assay. To evaluate the antitumor activity, HeLa cells were exposed to different concentrations of **1** and **2** for 24 h and their antiproliferative effect was determined by MTT assay [68]. Complex **2** exhibits much stronger cytotoxic effects than **1**. Antitumor performance of Cu^{II} ($Cu(ClO_4)_2{\cdot}6H_2O$) in 24 h was also investigated, and it did not induce changes compared to that of **1** and **2**. The antitumor activities are $Cu^{II} < \mathbf{1} < \mathbf{2}$. Heavy metal ions are cytotoxic to cells at 10^{-3} M [69]. Figure 6 shows that copper(II) exhibit antitumor activity at this level, but when copper(II) ions are diluted to 2×10^{-4} M, the percentage inhibition decreases sharply (IC_{50}) 2.30×10^{-4} M. Complex **2** kept its antitumor activity toward HeLa cells even at 10^{-6} M. To further evaluate the antitumor activity of **1** and **2**, IC_{50} values against HeLa cells were determined (table 2). The IC_{50} value of **2** is five-fold smaller than **1** due to the presence of 1,10-phenanthroline in **2**. Remarkably, it exhibits the

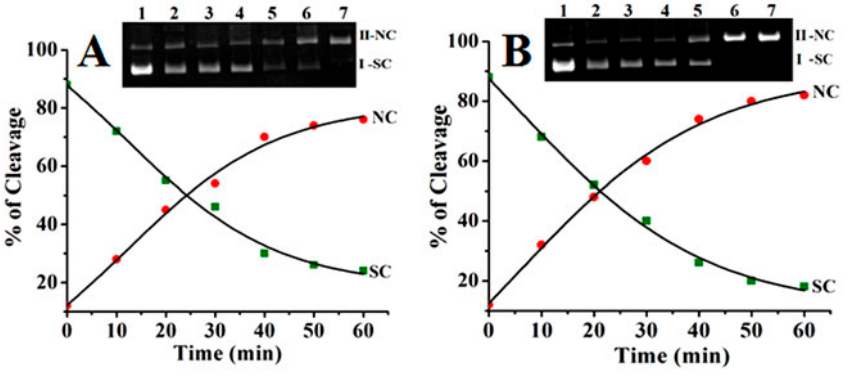

Figure 5. (A–B) Cleavage activity of **1** and **2** monitored by 0.8% agarose gel electrophoresis, where [DNA] (0.2 mg, 33 mM) and [Cu_2 complex] (30 μM). Time course measured in 10 mM Tris buffer, pH 7.5, 37 °C, showing the disappearance of supercoiled DNA (Form I) at (1) 0 min, (2) 10 min, (3) 20 min, (4) 30 min, (5) 40 min, (6) 50 min, and (7) 60 min (gel image showing supercoiled (Form I) and circular relaxed (Form II)).

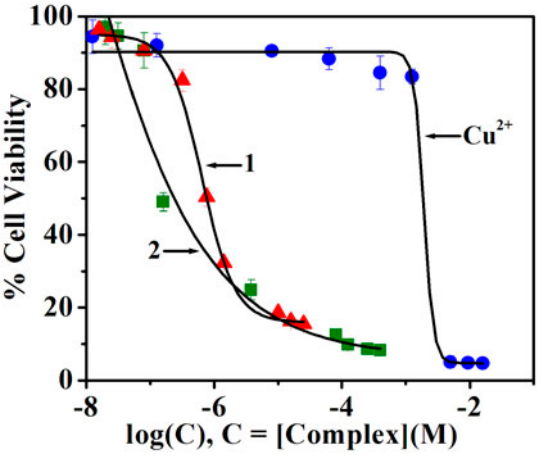

Figure 6. Inhibitory effect of copper(II), **1** and **2** on the proliferation of HeLa cells. Cells were exposed to the compounds for 24 h. The relative survival rate was determined in relation to that of untreated control cells, which was set to 100%. Data are means with standard deviation of three experiments and each experiment included triplicate wells.

highest activity against HeLa cells with an IC_{50} value of 15.82 μM, but smaller than cisplatin (IC_{50}, 3.80 μM) [70] against the same cell lines and under identical experimental conditions. Complex **2** exhibited high antiproliferative activity against HeLa cells *in vitro*, and can therefore be a candidate for further stages of screening *in vivo*.

3.4.2. Cell proliferation assay. Chemotherapy is a major therapeutic approach for localized and metastasized cancers. Complexes **1** and **2** at different concentrations (10, 20, 50, and 100 μM) were evaluated for *in vitro* cytotoxicity against human cervical carcinoma HeLa cancer cells by Trypan Blue exclusion method (figure 7). Screening results reveal that **1** and **2** inhibited 30 and 56% HeLa tumor cells at 10 μM, 44.6, and 80% at 20 μM, 56.6, and 100% at 50 μM and 59.8, and 100% at 100 μM concentrations, respectively. The macrocyclic dicopper(II) complexes **1** and **2** exhibit ligand-dependent increase in cytotoxicity to HeLa cells. The viability data agree with the IC_{50} values of **1** and **2** against HeLa cell line determined by using MTT assay.

3.4.3. LDH inhibition assay. The cytoplasmic enzyme (LDH), which catalyzes the oxidation of lactate to pyruvate and vice versa, is also a known marker of membrane integrity and a regulator of vital biochemical reactions [71]. The integrity and permeability of the plasma membrane were determined by measuring the amount of leakage of LDH from the cytoplasm. The quantity of LDH has been analyzed for HeLa cancer cell lysate as well as in conditioned media for 48 h treatment of **1** and **2**. The LDH was significantly decreased in cell lysate when compared to control cells with **1** and **2** treated cells (IC_{50} concentrations) (figure 8). The activity of LDH was significantly increased in conditioned media when compared with controlled cells, confirming the cytotoxic ability of **1** and **2** against HeLa cells. Because of the apoptosis induced by **1** and **2**, the membrane permeability increases, and hence there is leakage of LDH from the cells into the medium. Complex **2** caused

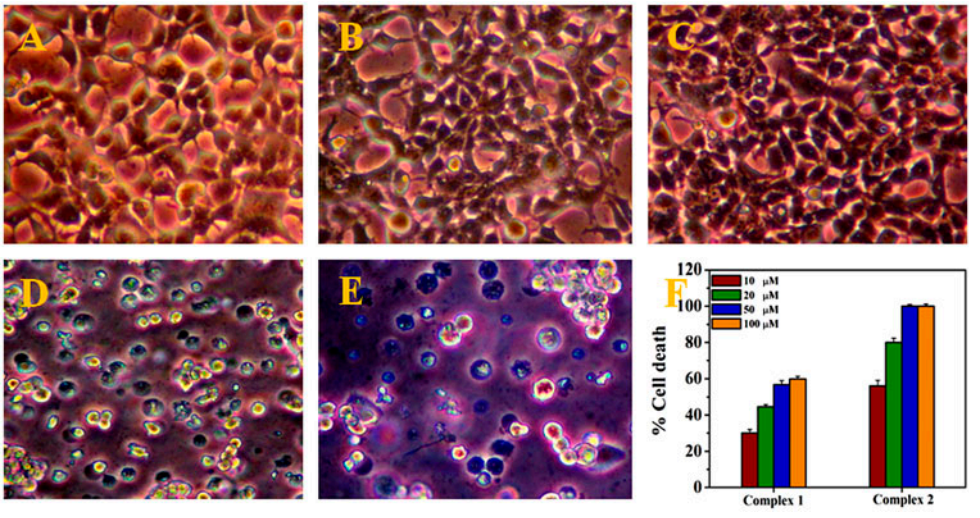

Figure 7. HeLa cells were separately cultured in the absence (A) or the presence (B, C, D, and E) of **1** and **2**. (A), control; (B, C), **1** (10 and 20 μM, respectively); (D, E), **2** (10 and 20 μM, respectively); (F), assessment of cell viability using the Trypan Blue exclusion assay.

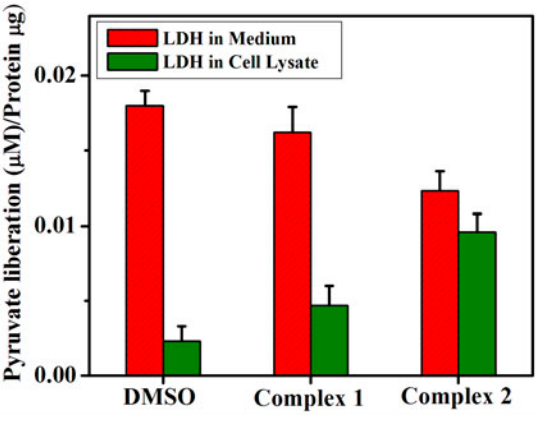

Figure 8. Cytotoxic effect of **1** and **2** in HeLa cells assessed by LDH activity in medium and cell lysate for 48 h.

significant LDH leakage ($p < 0.05$) as compared with **1** and control. This results in the content of LDH increasing in conditioned media and decreasing in the cell lysate.

4. Conclusion

A 1,10-phenanthroline containing Robson type macrocyclic dicopper(II) complex has been synthesized and characterized. X-ray crystallography reveals that 1,10-phenanthroline nitrogens strongly interact with copper(II) through coordinated water bridge. The analytical, UV–vis, ESI-MS, and EPR spectral data of **2** strongly support formation of phenanthroline coordinated complex in solution. Influence of 1,10-phenanthroline on DNA binding, DNA

cleavage, and cytotoxic properties of the Robson type macrocyclic dicopper(II) complex have been evaluated. The DNA binding and cleavage experiments suggest that **2** has better DNA binding and more efficient DNA cleavage than **1** under physiological conditions. Based on DNA experiments and cytotoxic data, we conclude that **2** has potential as a DNA-targeting agent in cancer chemotherapy. Additional work on the synthesis of aromatic ring extended phenanthroline-based dicopper(II) complexes and their biological studies are in progress.

Supplementary material

Crystallographic data (without structure factors) for the structure reported in this article have been deposited with the Cambridge Crystallographic Data Center, CCDC 736667. Copies of the data can be obtained free of charge from the CCDC (12 Union Road, Cambridge CB2 1EZ, UK; Tel: 27 (+44) 1223-336-408; Fax: (+44) 1223-336-003; E-mail: deposit@ccdc.cam.ac.uk; website http://www.ccdc.cam.ac.uk/products/csd/request). Supplemental data to this article can be accessed http://dx.doi.org/10.1080/00958972.2013.858136.

Acknowledgements

S.A. is grateful to CSIR, New Delhi, Government of India, for a fellowship (SRF). The authors thank the Department of Science and Technology (DST-FIST), New Delhi, Government of India, for financial support.

References

[1] K. Ghosh, P. Kumar, N. Tyagi, U.P. Singh, N. Goel. *Inorg. Chem. Commun.*, **14**, 489 (2011).
[2] C. Liu, M. Wang, T. Zhang, H. Sun. *Coord. Chem. Rev.*, **248**, 147 (2004).
[3] L.K.J. Boerner, J.M. Zaleski. *Curr. Opin. Chem. Biol.*, **9**, 135 (2005).
[4] X.-W. Li, Y. Yu, Y.-T. Li, Z.-Y. Wu, C.-W. Yan. *Inorg. Chim. Acta*, **267**, 64 (2011).
[5] M. Frezza, S.S. Hindo, D. Tomco, M.M. Allard, Q.C. Cui, M.J. Heeg, D. Chen, Q.P. Dou, C.N. Verani. *Inorg. Chem.*, **48**, 5928 (2009).
[6] E.R. Jamieson, S.J. Lippard. *Chem. Rev.*, **99**, 2467 (1999).
[7] S. Ramakrishnan, V. Rajendiran, M. Palaniandavar, V.S. Periasamy, B.S. Srinag, H. Krishnamurthy, M.A. Akbarsha. *Inorg. Chem.*, **48**, 1309 (2009).
[8] X.B. Yang, L. Wang, J. Zhang, Z.W. Zhang, H.H. Lin, L.H. Zhou, X.Q. Yu. *J. Enzyme Inhib. Med. Chem.*, **24**, 125 (2009).
[9] R. Hettich, H.-J. Schneider. *J. Am. Chem. Soc.*, **119**, 5638 (1997).
[10] A. Sreedhara, J.D. Freed, J.A. Cowan. *J. Am. Chem. Soc.*, **122**, 8814 (2000).
[11] J.-Z. Wu, L. Yuan, J.-F. Wu. *J. Inorg. Biochem.*, **99**, 2211 (2005).
[12] X. Cai, N. Pan, G. Zou. *Biometals*, **20**, 1 (2007).
[13] S. Ramakrishnan, D. Shakthipriya, E. Suresh, V.S. Periasamy, M.A. Akbarsha, M. Palaniandavar. *Inorg. Chem.*, **50**, 6458 (2011).
[14] T.K. Goswami, B.V.S.K. Chakravarthi, M. Roy, A.A. Karande, A.R. Chakravarty. *Inorg. Chem.*, **50**, 8452 (2011).
[15] M.H. Lim, I.H. Lau, J.K. Barton. *Inorg. Chem.*, **46**, 9528 (2007).
[16] L. Tjioe, T. Joshi, C.M. Forsyth, B. Moubaraki, K.S. Murray, J. Brugger, B. Graham, L. Spiccia. *Inorg. Chem.*, **51**, 939 (2012).
[17] S. Anbu, R. Ravishankaran, A.A. Karande, M. Kandaswamy. *Dalton Trans.*, 12970 (2012).
[18] S. Anbu, M. Kandaswamy, S. Kamalraj, J. Muthumarry, B. Varghese. *Dalton Trans.*, 7310 (2011).
[19] S. Anbu, S. Kamalraj, B. Varghese, J. Muthumary, M. Kandaswamy. *Inorg. Chem.*, **51**, 5580 (2012).
[20] S. Anbu, M. Kandaswamy. *Inorg. Chim. Acta*, **385**, 45 (2012).
[21] S. Anbu, S. Shanmugaraju, M. Kandaswamy. *RSC Adv.*, **2**, 5349 (2012).
[22] S. Anbu, M. Kandaswamy, P. Suthakaran, V. Murugan, B. Varghese. *J. Inorg. Biochem.*, **103**, 401 (2009).

[23] L. Leelavathy, S. Anbu, M. Kandaswamy, N. Karthikeyan, N. Mohan. *Polyhedron*, **28**, 903 (2009).
[24] S. Anbu, M. Kandaswamy. *Polyhedron*, **30**, 123 (2011).
[25] S. Anbu, M. Kandaswamy, M. Selvaraj. *Polyhedron*, **33**, 1 (2012).
[26] L.K. Thompson, S.K. Mandal, S.S. Tandon, J.N. Bridson, M.K. Park. *Inorg. Chem.*, **35**, 3117 (1996).
[27] Bruker–Nonius. *APEX–II and SAINT–Plus (Version 7.06a)*, Bruker AXS Inc., Madison, Wisconsin, USA (2004).
[28] SADABS. Bruker AXS Inc., Madison, Wisconsin, USA (1999).
[29] A. Altormare, G. Gascarano, C. Giacovazzo, A. Guagliardi. *J. Appl. Cryst.*, **26**, 343 (1996).
[30] J.C. King. *Practical Clinical Enzymology*, D. von Nostrand Co., London (1965).
[31] M. Thirumavalavan, P. Akilan, M. Kandaswamy. *Inorg. Chem.*, **42**, 3308 (2003).
[32] B. Jezowska, J. Lisowski, P. Chmielewski. *Polyhedron*, **7**, 337 (1988).
[33] S. Sharif, I.G. Shenderovich, L. Gonzalez, G.S. Denisov, D.N. Silverman, H.-H. Limbach. *J. Phys. Chem.*, **111**, 6084 (2007).
[34] S. Ramakrishnan, M. Palaniandavar. *J. Chem. Sci.*, **117**, 179 (2005).
[35] T. Hirohama, Y. Kuranuki, E. Ebina, T. Sugizaki, H. Arii, M. Chikira, P. Tamil Selvi, M. Palaniandavar. *J. Inorg. Biochem.*, **99**, 1205 (2005).
[36] R. Carballo, B. Covelo, S. Balboa, A. Casteneiras, J. Nicklos. *Z. Anorg. Allg. Chem.*, **627**, 948 (2001).
[37] M. Vaidyanathan, M. Palaniandavar. *Proc. Indian Acad. Sci.*, (Chem. Sci.) **112**, 223 (2000).
[38] U. Sakaguchi, A.W. Addison. *J. Chem. Soc., Dalton Trans.*, 600 (1978).
[39] B.J. Hathaway. *Comprehensive Coordination Chemistry*, Pergamon Press, Oxford, Vol. 5, p. 533 (1987).
[40] V. Uma, M. Kanthimathi, T. Weyhermuller. B. Unni Nair, *J. Inorg. Biochem.*, **99**, 2299 (2005).
[41] P.K. Sasmal, A.K. Patra, M. Nethaji, A.R. Chakravarty. *Inorg. Chem.*, **45**, 11112 (2007).
[42] J.B. Le Pecq, C. Paoletti. *J. Mol. Biol.*, **27**, 87 (1967).
[43] Y. Mei, J.J. Zhou, H. Zhou, Z.Q. Pan. *J. Coord. Chem.*, **65**, 643 (2012).
[44] X.-L. Wang, M. Jiang, Y.-T. Li, Z.-Y. Wu, C.-W. Yan. *J. Coord. Chem.*, **66**, 1985 (2013).
[45] S.-H. Cui, M. Jiang, Y.-T. Li, Z.-Y. Wu, X.-W. Li. *J. Coord. Chem.*, **64**, 4209 (2011).
[46] C. Gao, X. Ma, J. Lu, Z. Wang, J. Tian, S. Yan. *J. Coord. Chem.*, **64**, 2157 (2011).
[47] H.H. Lu, Y.T. Li, Z.Y. Wu, K. Zheng, C.W. Yan. *J. Coord. Chem.*, **64**, 1360 (2011).
[48] H.L. Wu, X.C. Huang, B. Liu, F. Kou, F. Jia, J.K. Yuan, Y. Bai. *J. Coord. Chem.*, **64**, 4383 (2011).
[49] K. Pothiraj, T. Baskaran, N. Raman. *J. Coord. Chem.*, **65**, 2110 (2012).
[50] R. Rao, A.K. Patra, P.R. Chetana. *Polyhedron*, **27**, 1343 (2008).
[51] R.F. Pasternack. *Chirality*, **15**, 329 (2003).
[52] D.G. Dalgleish, M.C. Feil, A.R. Peacocke. *Biopolymers*, **11**, 2415 (1972).
[53] S. Mahadevan, M. Palaniandavar. *Inorg. Chem.*, **37**, 693 (1998).
[54] P.U. Maheswari, M. Palaniandavar. *J. Inorg. Biochem.*, **98**, 219 (2004).
[55] E. Nyarko, N. Hanada, A. Habib, M. Tabata. *Inorg. Chim. Acta*, **357**, 739 (2004).
[56] M. Lee, A.L. Rhodes, M.D. Wyatt, S. Forrow, J.A. Hartley. *Biochemistry*, **32**, 4237 (1993).
[57] Y. Zhao, J. Zhu, W. He, Z. Yang, Y. Zhu, Y. Li, J. Zhang, Z. Guo. *Chem. Eur. J.*, **12**, 6621 (2006).
[58] W. Qian, F. Gu, L. Gao, S. Feng, D. Yan, D. Liao, P. Cheng. *Dalton Trans.*, 1060 (2007).
[59] J.K. Barton, A.C. Raphael. *J. Am. Chem. Soc.*, **106**, 2466 (1984).
[60] N. Grover, N. Gupta, P. Singh, H.H. Thorp. *Inorg. Chem.*, **31**, 2014 (1992).
[61] J.M. Veal, R.L. Rill. *Biochemistry*, **30**, 1132 (1991).
[62] P.P. Pellegrini, J.R. Aldrich-Wright. *Dalton Trans.*, 176 (2003).
[63] X. Sheng, X. Guo, X.M. Lu, G.Y. Lu, Y. Shao, F. Liu, Q. Xu. *Bioconjugate Chem.*, **19**, 490 (2008).
[64] L.M. Rossi, A. Neves, A.J. Bortoluzzi, R. Horner, B. Szpoganicz, H. Terenzi, A.S. Mangrich, E.P. Maia, E.E. Castellano, W. Haase. *Inorg. Chim. Acta*, **358**, 807 (2005).
[65] M.C.B. Oliveira, M.S.R. Couto, P.C. Severino, T. Foppa, G.T.S. Martins, B. Szpoganicz, R.A. Peralta, A. Neves, H. Terenzi. *Polyhedron*, **24**, 495 (2005).
[66] D.J. Wright, W.E. Jack, P. Modrich. *J. Biol. Chem.*, **274**, 31896 (1999).
[67] N.P. Stanford, S.E. Halford, G.S. Baldwin. *J. Mol. Biol.*, **288**, 105 (1999).
[68] M.C. Alley, D.A. Scudiero, A. Monks, M.L. Hyrsey, M.J. Czerwinski, D.L. Fine, B.J. Abbott, J.G. Mayo, R.H. Shoemaker, M.R. Boyd. *Cancer Res.*, **48**, 589 (1988).
[69] F. Liang, C. Wu, H. Lin, T. Li, D. Gao, Z. Li, J. Wei, C. Zheng, M. Sun. *Bioorg. Med. Chem. Lett.*, **13**, 2469 (2003).
[70] J. Wesierska-Gadek, M.P. Kramer, G. Schmid. *J. Cell. Biochem.*, **104**, 189 (2008).
[71] R.K. Murray, D.K. Granner, P.A. Mayes, V.W. Rodwell. *Harper's Illustrated Biochemistry*, Lange Medical Books, New Delhi (2003).